Biophysical Chemistry 252 (2019) 106207

Contents lists available at ScienceDirect

Biophysical Chemistry

journal homepage: www.elsevier.com/locate/biophyschem

Research Article

Structural and dynamic responses of calcium ion binding loop residues in metallo-proteins

Samapan Sikdar[a,*], Mahua Ghosh[a], Arunava Adak[a], J. Chakrabarti[a,b,*]

[a] Department of Chemical, Biological & Macro-Molecular Sciences, S. N. Bose National Centre for Basic Sciences, Sector III, Block JD, Salt Lake, Kolkata 700106, India
[b] The Thematic Unit of Excellence on Computational Materials Science, S. N. Bose National Centre for Basic Sciences, Sector III, Block JD, Salt Lake, Kolkata 700106, India

HIGHLIGHTS

- Frequent presence of multiple dihedral isomeric states in apo-compared to holo-state.
- Dihedral relaxation is slower for low barrier heights separating isomeric states.
- Low barrier heights enhances barrier re-crossing frequency.
- Slow decay of dihedral fluctuations due to more frequent barrier crossing events.
- Presence of multiple dihedral isomeric states slows down macro-scale fluctuations.

GRAPHICAL ABSTRACT

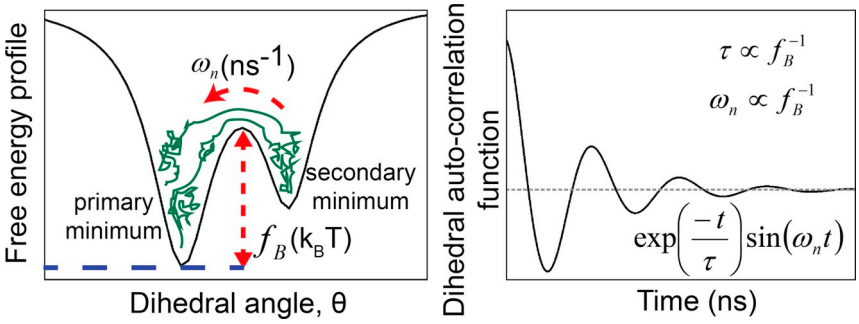

ARTICLE INFO

Keywords:
Langevin equation
Molecular dynamics
Dihedral conformational transitions
Barrier crossing
Dihedral relaxation time-scale
Calcium binding proteins

ABSTRACT

Conformational changes in bio-molecular systems are fundamental to several biological processes. It is important to study changes in responses of underlying microscopic variables, like dihedral angles as conformational change takes place. We perform all-atom simulations and modelling via Langevin equation to illustrate the changes in structural and dynamic responses of dihedral angles of calcium ion binding residues of different proteins in metal ion free (apo) and bound (holo) states. The equilibrium distributions of dihedral angles in apo- and holo-states represent structural response. Our studies show the presence of dihedrals with multiple peaks (isomeric states) separated by barrier heights is more frequent in apo- than in holo-state. The relaxation time-scale of dihedral fluctuations is found to increase linearly with decreasing barrier height due to more frequent barrier re-crossing events. The slow kinetic response of the dihedrals also contributes to slowing down of macro-scale fluctuations, which may be useful to understand kinetics of various bio-molecular processes.

1. Introduction

Bio-molecules like proteins, typically adopt different conformations upon ligand binding. Conformational changes in various bio-molecular systems, like many protein-ligand complexes, are well characterized both experimentally [1–5] and theoretically in terms of different models [6–9] and play vital role in governing allostery, function and evolution [10]. Large bio-molecules have many internal degrees of freedom. For instance, the dihedral angles defined by atomic planes [9,11–15], are microscopic variables to study conformational changes in a protein. The changes in structural and dynamical properties of these underlying microscopic variables accompanying conformational

* Corresponding authors.
E-mail addresses: sikdarsamapan.acad@gmail.com, samapans@imsc.res.in (S. Sikdar), jaydeb@bose.res.in (J. Chakrabarti).

https://doi.org/10.1016/j.bpc.2019.106207
Received 25 March 2019; Received in revised form 11 June 2019
Available online 20 June 2019

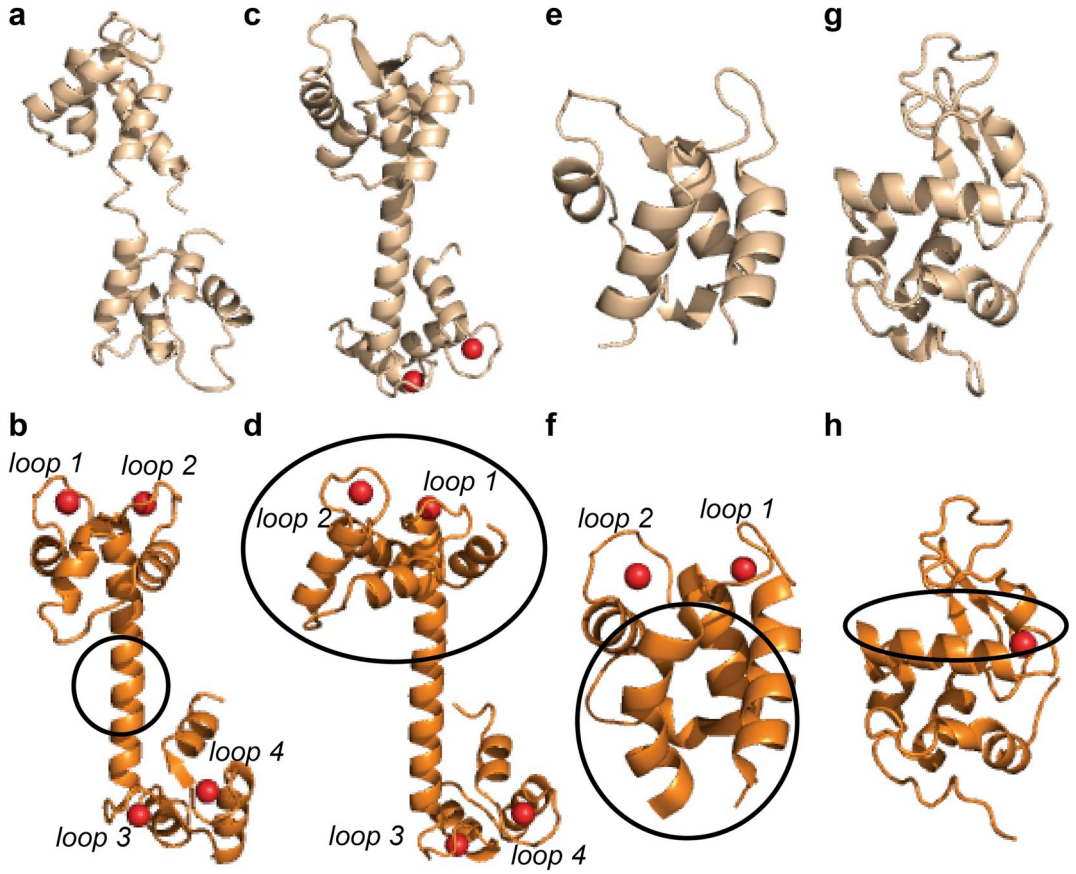

Fig. 1. The structures of Ca^{2+} binding proteins used in this study. (a) apo-CaM (PDB id: *1CFD*), (b) holo-CaM (PDB id: *1CLL*), (c) apo-TnC (PDB id: *1TOP*), (d) holo-TnC (PDB id: *1YTZ*), (e) apo-CALB (PDB id: *1CLB*), (f) holo-CALB (PDB id: *4ICB*), (g) apo-aLA (PDB id: *1F6R*) and (h) holo-aLA (PDB id: *1F6S*). The bound Ca^{2+} ions are shown in red. CaM undergoes collapsed to extended conformation owing to conformational changes in central linker, TnC shows rearrangement of helices at N-domain (circled in black) upon Ca^{2+} ion binding. Similar helix re-orientation (circled in black) is observed for CALB. aLA exhibits closing of interfacial cleft (circled in black) upon Ca^{2+} ion binding. (For interpretation of the references to colour in this figure legend, the reader is referred to the web version of this article.)

changes are not well studied so far, even though such changes form the basis of microscopic description of kinetics of different processes.

We consider microscopic responses of residues in calcium (Ca^{2+}) ion binding loops of different proteins in aqueous medium. These proteins include: Calmodulin (CaM) [16] mediating muscle contraction, inflammation, metabolism, cytoskeleton movement etc.; calbindin (CALB) [17,18] a vitamin D responsive protein found in intestine and kidney; Troponin C (TnC) [19] of troponin complex responsible for activating muscle contraction; and alpha-Lactalbumin (aLA) [20], a milk protein participating in lactose synthesis and fatty acid binding. The crystal structures of these proteins are known both in Ca^{2+} free (apo) and bound (holo) states, as shown in Fig. 1. The apo-CaM conformation is collapsed owing to flexible central helix. Upon Ca^{2+} binding the central helix becomes rigid and holo-CaM shows an extended conformation. TnC and CALB undergo 'closed' to 'open' conformation due to helix re-arrangement, while the interfacial cleft of aLA narrows down upon Ca^{2+} ion binding.

The residues of Ca^{2+} binding loops are shown in Table 1, the coordinating ones being highlighted. Both CaM and TnC have an N- and a C-terminal domain separated by a linker helix. Each of these domains possesses a pair of 12-residue long Ca^{2+} binding loops. CALB possesses two loops: a 14-residue loop 1 and another 12-residue loop 2, while the Ca^{2+} binding loop of aLA comprises of ten residues. All the loops are rich in acidic and polar residues so that the metal ion has primarily electrostatic interactions with the loop residues.

Ca^{2+} binding to CaM and consequent conformational changes have been studied in details through different experiments, like time resolved fluorescence spectroscopy, NMR, grafting approach [1,5,21–26]. These studies indicate that N- and C-terminal domains of CaM bear significant difference in the energetics of Ca^{2+} binding. The C-terminal domain has 6 to 10-fold higher affinity for Ca^{2+} ion [5,24,25]. Hence, loop 3 and loop 4 in C– terminal of CaM gets saturated completely before N-terminal loop 1 and loop 2 begin to be occupied. Although domain specific Ca^{2+} binding affinities are largely different, the two CaM-domains share a high degree of sequence homology (~ 75%) [27–29]. The differential binding affinity indicates that the microscopic variables associated with Ca^{2+} ion binding behave differently at the two domains.

Such observations lead us to study structural and dynamic properties of backbone dihedral angles φ and ψ of residues from ion binding loops in apo- and holo-states. We perform all-atom molecular dynamics simulations separately on each protein in both states starting from their known crystal structures, keeping the ensembles same. The equilibrium structural responses are given on comparing dihedral distributions and the dynamic responses from their relaxation time scales in these two states. We observe that the backbone dihedral distributions are mostly single peaked in both states. However, there are multiple peaked distributions, which are more in the apo- than in the holo-state. The peaks are indicative of isomeric states [30] separated by barriers, giving rise to different isomerisation patterns. The dihedral relaxation is slower in presence of multiple peaks: the lower is the barrier height; the slower is its relaxation. We explain this through mathematical modelling based on the Langevin equation [31,32] for dihedral fluctuations. The mathematical modelling shows that barrier re-crossing between isomeric states is more frequent for low barrier heights. Such frequent barrier re-crossing events over small barriers back to the initial dihedral

Table 1
The residues in Ca^{2+} ion binding loops of different proteins. The coordinating residues are indicated in bold-face.

Loop position													
I	II	**III**	IV	**V**	VI	**VII**	VII	IX	X	XI	**XII**	XIII	XIV
CaM loop 1													
D20	K21	**D22**	G23	**D24**	G25	**T26**	I27	T28	T29	K30	**E31**		
CaM loop 2													
D56	A57	**D58**	G59	**N60**	G61	**T62**	I63	D64	F65	P66	**E67**		
CaM loop 3													
D93	K94	**D95**	G96	**N97**	G98	**Y99**	I100	S101	A102	A103	**E104**		
CaM loop 4													
D129	G130	**D131**	G132	**D133**	G134	**Q135**	V136	N137	Y138	E139	**E140**		
TnC loop 1													
D29	A30	**D31**	G32	**G33**	G34	**D35**	I36	S37	T38	K39	**E40**		
TnC loop 2													
D65	E66	**D67**	G68	**S69**	G70	**T71**	I72	D73	F74	E75	**E76**		
CALB loop 2													
D54	K55	**N56**	G57	**D58**	G59	**E60**	V61	S62	F63	E64	**E65**		
CALB loop 1													
A14	A15	K16	**E17**	G18	**D19**	P20	N21	**Q22**	L23	S24	K25	E26	**E27**
aLA loop													
K79	F80	L81	**D82**	D83	**D84**	L85	T86	**D87**	**D88**				

isomeric state renders the dihedral relaxation slower. Moreover, the presence of backbone dihedral angles of the Ca^{2+} binding loops with multiple isomeric states governs the fluctuation behaviour of these loops. The more is the number of such dihedrals possessing multiple isomeric states, the slower is the loop's relaxation. This is also due to the event of barrier crossing between different isomeric states that slows down the relaxation time-scale of loop fluctuations.

2. Methods

2.1. Simulation details

The MD simulations using standard force field, CHARMM27 [33] are performed for both Ca^{2+} ion free (apo) and bound (holo) proteins, namely calmodulin (PDB id: 1CFD, 1CLL) [34], calbindin (1CLB, 4ICB) [17,18], skeletal muscle Troponin C (1TOP, 1YTZ) [19] and alpha-Lactalbumin (1F6R, 1F6S) [20]. The simulations are performed in presence of explicit water (TIP3P water model) and counter-ions with NAMD [35] package at 310 K and 1 atm pressure in isothermal-isobaric (*NPT*) ensemble using the periodic boundary conditions and 1 femto-second time-step. The long ranged electrostatic interactions are treated by particle-mesh Ewald method. We perform an energy minimization of 1000 steps and then run 200 nanoseconds (ns) long simulations. The analysis is performed on the last 100 ns equilibrated trajectories.

2.2. Analysis

The radius of gyration, $R_g = \left[\sum_i m_i(\vec{r_i} - \vec{R}_{CM})^2 / \sum_i m_i\right]^{\frac{1}{2}}$ of different Ca^{2+} binding loops is calculated as the average distance of loop C-α atoms from their centre of mass ($\vec{R}_{CM}$), $\vec{R}_{CM} = \sum_i m_i \vec{r_i} / \sum_i m_i$, where $m_i$and $\vec{r_i}$ are the mass and position vectors of the i^{th} C-α atom.

The normalized dihedral auto-correlation function in time is defined as $C(\theta, t)$.

$$C(\theta, t) = \frac{\langle(\cos\theta(t_0 + t) - \langle\cos\theta\rangle)(\cos\theta(t_0) - \langle\cos\theta\rangle)\rangle}{\langle(\cos\theta(t_0) - \langle\cos\theta\rangle)^2\rangle} \quad (1)$$

The terms, $cos\theta(t_0)$ and $cos\theta(t_0 + t)$ represent cosine values of the dihedral θ at some initial time t_0 and after some time interval t respectively, while $\langle cos\theta\rangle$is the time-averaged cosine value of the dihedral angle [31,32]. The outer angular brackets indicate averaging over the initial conditions chosen from the equilibrated trajectory. Above notations remaining same, the normalized auto-correlation function of R_g in time is given by, $C(R_g, t) = \frac{\langle(R_g(t_0+t) - \langle R_g\rangle)(R_g(t_0) - \langle R_g\rangle)\rangle}{\langle(R_g(t_0) - \langle R_g\rangle)^2\rangle}$.

3. Results

3.1. Simulation results

The equilibrations of the systems are judged from saturation of root mean squared deviations (RMSD) of backbone C-α atoms. We compute the structural response from distributions of backbone dihedral angles,φ and ψ for all loop residues over equilibrated trajectories. The Ramachandran plots (SI Fig.S1) indicate that secondary structural elements of the loop residues do not change in apo and holo-states. We also compute the dynamical properties in terms of dihedral auto-correlation function (DACF) [31] which indicates how long a change in a dihedral angle takes to relax.

3.2. Dihedral distributions

We examine the distributions $p_R{}^i(\theta)$ of dihedral θ for residue R in protein "i" in both apo- and holo-state conformations. The global maximum of the distribution is defined as primary peak, while local maxima if present are considered as secondary peaks provided their peak height is at least 10% of the primary one. The peaks $p_R{}^i(\theta)$ of the backbone dihedral angles represent isomeric states [30,36] (Fig. 2). For instance, ${p_{A103}}^{CaM}(\varphi)$ (Fig. 2a) exhibits overlapping unimodal distributions in both apo- and holo-state indicating same isomeric state in two cases. ${p_{D65}}^{TnC}(\psi)$ (Fig. 2b) is also unimodal in both apo- and holo-states but represent two different isomeric states. On other hand, ${p_{D20}}^{CaM}(\varphi)$ (Fig. 2c) exhibits bimodal apo-state distribution with a larger peak at -117.5° and a smaller peak at -62.5°. The presence of two distinct isomeric states with finite population is indicative of isomeric transitions in the apo-state. However, in holo-CaM the distribution has a single peak at -62.5°, showing a single isomeric state. The side-chain dihedrals show different behaviour where both apo- and holo-state distributions are multimodal, indicative of different rotameric states [37]. Additional data on dihedral distributions indicating isomeric and rotameric states are illustrated in SI Fig. S2 (a-e).

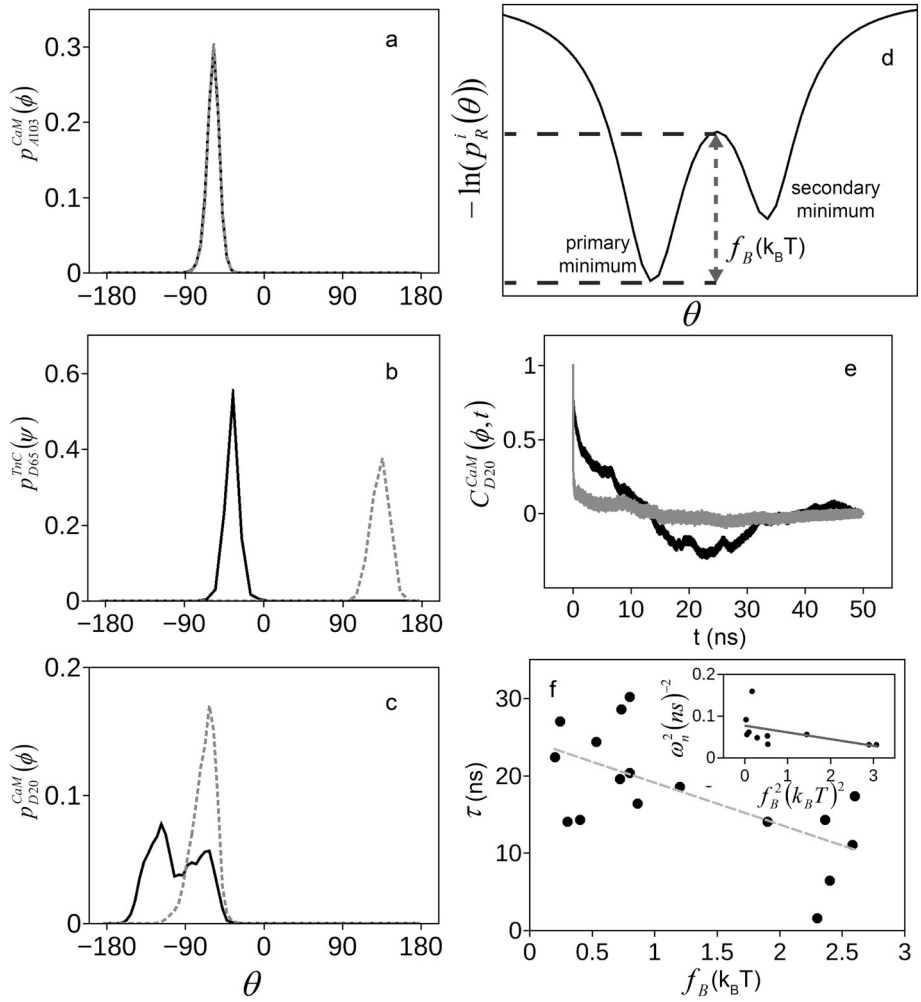

Fig. 2. The equilibrium distributions, $p_R{}^i(\theta)$ of dihedral angles "θ" of residue "R" in protein "i" for apo (solid black line) and holo (dashed gray line). (a) $p_{A103}{}^{CaM}(\varphi)$, (b) $p_{D65}{}^{TnC}(\psi)$, (c) $p_{D20}{}^{CaM}(\varphi)$. (d) Schematic showing barrier height separating dihedral isomeric states. (e) The DACF response, $C_{D20}{}^{CaM}(\varphi,t)$ illustrating different time-scales for apo (black) and holo (gray) states. (f) Correlation plot of barrier height, f_B with overall decay time constant τ. Inset shows correlation plot of $f_B{}^2$ with $\omega_n{}^2$.

Table 2
Number of single- and multi-peaked backbone dihedral distributions for each loop in apo-state: $N_{SP}{}^{apo}$, $N_{MP}{}^{apo}$ and in holo state:$N_{SP}{}^{holo}$, $N_{MP}{}^{holo}$.

	Apo		Holo	
	$N_{SP}{}^{apo}$	$N_{MP}{}^{apo}$	$N_{SP}{}^{holo}$	$N_{MP}{}^{holo}$
CaM loop 1	16	8	23	1
CaM loop 2	19	5	24	0
CaM loop 3	23	1	24	0
CaM loop 4	22	2	23	1
TnC loop 1	21	3	20	4
TnC loop 2	12	12	19	5
CALB loop 1	18	10	22	6
CALB loop 2	19	5	18	6
aLA loop	18	2	19	1

The numbers of single- and multi-peaked backbone dihedral distributions in apo-state, represented as $N_{SP}{}^{apo}$, $N_{MP}{}^{apo}$ and similarly $N_{SP}{}^{holo}$, $N_{MP}{}^{holo}$ in holo-states for each loop are shown in Table 2. $N_{MP}{}^{apo}$ is significantly high for CaM loop 1 and loop 2, TnC loop 2 and both CALB loops. However, the backbone dihedral distributions in holo-state are predominantly single peaked with few exceptions, like TnC and CALB loops, where $N_{MP}{}^{holo}$ is high. Overall the number of multiple peaked distributions is less in the holo-state compared to the apo. Moreover, presence of multi-peaked dihedral distributions in the apo-state varies non-uniformly between different loops of the same protein.

The equilibrium dihedral distributions $p_R{}^i(\theta)$ can be associated to free energy profiles, given by $-\ln(p_R{}^i(\theta))$ in units of k_BT (schematically shown in Fig. 2d). Let us consider a bimodal dihedral distribution. The corresponding free energy profile has a primary minimum corresponding to major population of the distribution and a secondary minimum corresponding to minor population. The barrier height separating primary minimum from secondary minimum, f_B in units of k_BT, is estimated from the free energy profile as shown in Fig. 2d. The estimated barrier heights corresponding to bimodal backbone dihedral distributions of apo-states are summarized in SI Table S1.

3.3. Dihedral auto-correlation functions

The dynamical features of the dihedral angles are extracted from the DACF (see Eq. (1) in Methods section). The t dependence of DACF $C_R{}^i(\theta,t)$ of dihedral θ for residue R in protein "i" in apo- or holo-state depends on the number of isomeric states. The DACF for $C_{D20}{}^{CaM}(\varphi,t)$ (Fig. 2e) in apo- and holo-state is shown as a representative case. The apo-state distribution, $p_{D20}{}^{CaM}(\varphi)$ (in Fig. 2c) being multiple peaked; the auto-correlation amplitude is characterized by initial slow decay along with significant anti-correlation at long time. However, in holo-state, the equilibrium distribution is single peaked and $C_{D20}{}^{CaM}(\varphi,t)$ shows fast decay. This observation holds true for other cases as well.

More data on DACFs are shown in SI Figs. S2 (f-j), S3 and S4. The DACFs corresponding to multimodal distributions bear signature of damped oscillations [31,32]. Consequently, we fit the apo-state DACFs from simulation for different cases with a functional form, $exp\left(\frac{-t}{\tau}\right) sin(\omega_n t)$, characterized by an oscillation frequency, ω_n and an overall decay time constant,τ. We treat ω_n and τ as parameters for best fit. The best fitted parameters are shown in SI Table S1. The DACFs, $C_R^i(\theta,t)$ calculated from simulation data have maximum lag-time, 't' = 50 ns. We do not consider data points with τ close to the maximum lag-time. The correlation plot of f_B versus τ is shown in Fig. 2f with τ up to 35 ns. The correlation coefficient ~ -0.64 indicating that τ decreases linearly with increasing f_B. The inset shows that ${\omega_n}^2$ decreases linearly with ${f_B}^2$.

3.4. Loop size fluctuations

We consider fluctuations in large scale properties of these Ca^{2+} binding loops in both apo- and holo-states, by calculating its radius of gyration (R_g). R_g, a measure of loop size, is given by the average distances of C-α atoms of loop residues (as shown in Table 1) from their centre of mass. We examine the equilibrium distributions, $P(R_g)$ of different Ca^{2+} ion binding loops in both states (Fig. 3). The peaks of these distributions are defined in a similar manner as in the dihedral distributions and summarized in SI, Table S2. The $P(R_g)$ of CaM loop 1 (Fig. 3a) shows a bimodal apo-state distribution with a major peak and a minor peak. The holo-state distribution, in contrast, shows a single sharp peak in vicinity of the apo-state minor peak. The equilibrium R_g distributions of apo-CaM loop 2 (Fig. 3b) is single-peaked with an extended tail towards higher R_g values, while in the holo-state, the peak shifts towards lower R_g. The $P(R_g)$ of loop 3 (Fig. 3c) and loop 4 (Fig. 3d) of CaM are unimodal in both states, with mean R_g albeit lower in the holo-state compared to the apo. Similarly, the apo- and the holo-state $P(R_g)$ of both TnC loop 1 (Fig. 3e) and TnC loop 2 (Fig. 3f) indicate decrease in R_g values upon Ca^{2+} ion binding. The $P(R_g)$ of CALB loop 1 (Fig. 3g) in the apo-state is bimodal and shows a maximum with a shoulder. The corresponding holo-state peak is at a lower R_g value with a tail extending towards the apo-population. The apo-state $P(R_g)$ of CALB loop 2 (Fig. 3h) is characterized by a single peak, while the holo-state exhibits a primary maximum and another secondary peak. In contrast, the equilibrium R_g distributions of aLA (Fig. 3i) loop have sharp and single peaked $P(R_g)$ in both states. Overall the Ca^{2+} bound loops are smaller and more compact in structure than in the apo-state of all the proteins. This is due to strong electrostatic interaction between the acidic residues of the loops with the Ca^{2+} ion. Thus, the loop sizes depend uniquely on conformational state of the protein.

The decay timescales of R_g fluctuations are estimated from the time-correlation functions, $C(R_g,t)$ (see Methods section) of these Ca^{2+} ion binding loops in both states (Fig. 4). The $C(R_g,t)$ data is fitted with the same functional form as the DACF earlier, to yield characteristic decay time-scale,τ_{Rg}, summarized in SI, Table S2. The dynamic response, $C(R_g,t)$ of CaM loop 1 (Fig. 4a) and loop 2 (Fig. 4b) indicate slow decay and long-time anti-correlation in the apo-state. In the holo-state, the fluctuations in $C(R_g,t)$ of both loops die down quickly within pico-second timescale. The $C(R_g,t)$ of CaM loop 3 (Fig. 4c) decay relatively faster in both states. In contrast, both the apo- and the holo-state $C(R_g,t)$ of CaM loop 4 (Fig. 4d) show significant anti-correlation and slow decay. The relaxation time-scales, τ_{Rg} of TnC loop 1 (Fig. 4e) are similar in both states, while the fluctuations in apo-TnC loop 2 decay slowly than that in the holo-state (Fig. 4f). Similarly, the fluctuations of CALB loop 1 (Fig. 4g) also exhibit slower relaxation in the apo-state compared to the holo-state. On other hand, the $C(R_g,t)$ of CALB loop 2 is characterized by slow decay in both the apo- and the holo-states (Fig. 4h). In contrast aLA loop exhibits fast relaxation time-scales (Fig. 4i) in both states.

Next, we probe connection between macro-scale and micro-scale fluctuations by correlating the time-scales of loop size fluctuations with equilibrium dihedral distributions. We correlate to this end, the time-scale, τ_{Rg} of loop dynamics in both the apo- and the holo-states to the number of multi-peaked dihedral distributions ${N_{MP}}^{apo}$ and ${N_{MP}}^{holo}$ of each loop. The resulting scatter-plot in Fig. 5 shows good linear correlation of 0.76, indicating that larger the number of multi-peaked dihedral distributions, the slower is the relaxation of loop fluctuations. Thus loop size fluctuations are concomitant with isomeric transitions of dihedral angles.

3.5. Mathematical model

We account for the slowing down of relaxation of the dihedral angles with decreasing barrier heights, separating the isomeric states through a simple stochastic model. Let us consider a double minima free energy profile in the mathematical modelling consistent with a bimodal distribution in the dihedral space. The schematic is shown in

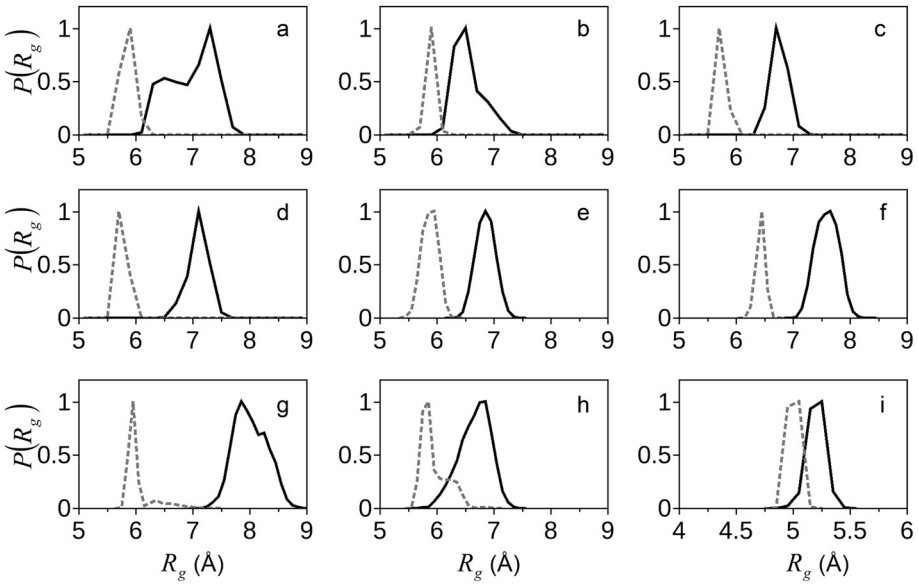

Fig. 3. The equilibrium distributions of radius of gyration, $P(R_g)$of (a) CaM loop 1, (b) CaM loop 2, (c) CaM loop 3, (d) CaM loop 4, (e) TnC loop 1, (f) TnC loop 2, (g) CALB loop 1, (h) CALB loop 2 and (i) aLA loop in apo (black line) and holo (gray line) states.

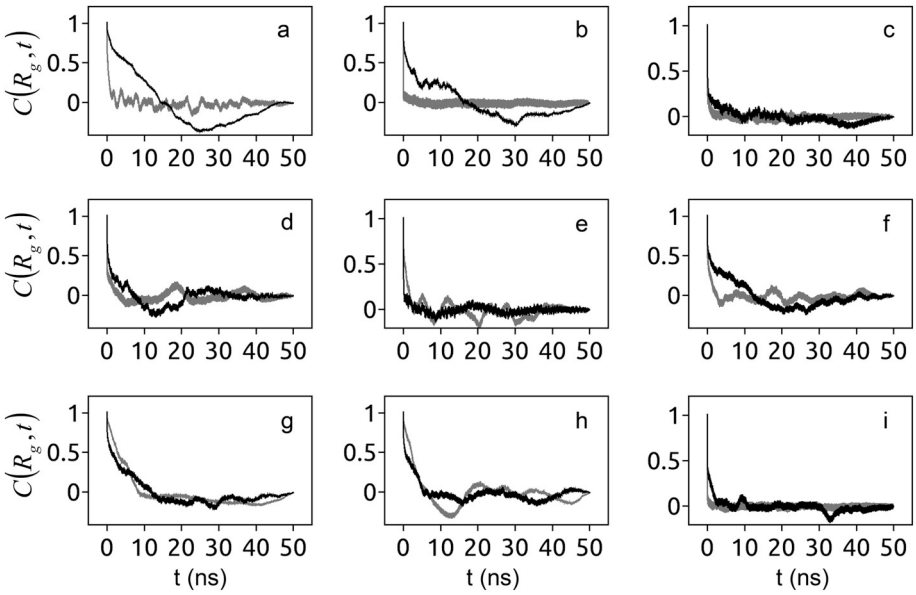

Fig. 4. The time-correlation function, $C(R_g,t)$ of (a) CaM loop 1, (b) CaM loop 2, (c) CaM loop 3, (d) CaM loop 4, (e) TnC loop 1, (f) TnC loop 2, (g) CALB loop 1, (h) CALB loop 2 and (i) aLA loop in apo (black line) and holo (gray line) states.

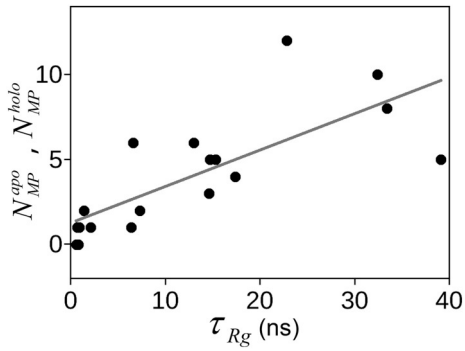

Fig. 5. Scatter-plot showing correlation between τ_{Rg} and number of multi-peaked backbone dihedral distributions $N_{MP}{}^{apo}$ (in apo-state) and $N_{MP}{}^{holo}$ (in holo-state) of each loop.

Fig. 2d. The primary free energy minimum corresponds to the major peak of dihedral distribution. The dihedral angle undergoes isomerisation by transition from the primary free energy minimum to the secondary one separated by a barrier,f_B. The dynamics of dihedral angles is modelled through the Langevin equation of a damped oscillator [31,32].

$$I\ddot{\theta} + \frac{f_B}{\omega_0}\dot{\theta} + k\theta(t) = f(t) \tag{2}$$

where, $\theta(t)$ is the torsional displacement, I is the moment of inertia about the torsional axis. The torque is $-k\theta$ where the force constant k is given by the inverse width of free energy profile at the primary minimum. The barrier hinders the dihedral motion which can be considered as frictional force, given by $\Gamma_0 = \frac{f_B}{\omega_0}$ where ${\omega_0}^{-1}$ is a typical time-scale associated with the attempts to cross the barrier. The $f(t)$ is thermal noise considered to have Gaussian statistics with zero mean and variance $\frac{k_BT}{I\omega_0}\delta(t)$. Taking the Fourier transform of Eq. (2) yields $\theta(\omega)$ and the DACF in the frequency domain:

$$\langle\theta(\omega)\theta(-\omega)\rangle = \frac{\langle f(\omega)f(-\omega)\rangle}{(k - I\omega^2)^2 + \left(\frac{\omega f_B}{\omega_0}\right)^2} \tag{3}$$

The inverse Fourier transform of Eq. (3) yields:

$$\langle\theta(t)\theta(0)\rangle = \int_{-\infty}^{+\infty} \frac{exp(-i\omega t)}{(k - I\omega^2)^2 + \left(\frac{\omega f_B}{\omega_0}\right)^2} d\omega \tag{4}$$

From Eq. (4) we obtain,

$$\langle\theta(t)\theta(0)\rangle = Asin\left(\sqrt{1 - \left(\frac{f_B}{2I\omega_0}\right)^2}\,\omega_0 t\right) exp\left(-\frac{f_B}{2I\omega_0}t\right)$$
$$= Asin(\omega_n t)\, exp\left(\frac{-t}{\tau}\right) \tag{5}$$

This form is consistent with the simulation data. The exponential term indicates overall decay of the DACFs, with time scale, $\tau = \frac{2k}{f_B\omega_0}$having inverse dependence on f_B as found in the simulations. The barrier re-crossing between secondary minimum to primary minimum leads to an oscillatory form of the correlation within a decaying envelope. The oscillation frequency $\omega_n = \sqrt{1 - \left(f_B/_{2k}\right)^2}\,\omega_0$ represents the barrier re-crossing frequency, which is real as long as $f_B < 2k$ and decreases with increasing f_B. Larger barrier suppresses the barrier re-crossing in agreement to simulation data (see inset of Fig. 2f). Since, $\omega_n = \sqrt{\omega_0^2 - \left(\frac{1}{\tau}\right)^2}$, so increase in τ results in enhanced barrier re-crossing frequency. In other words, frequent barrier crossing events between two isomeric states leads to slow decay of the DACF. Further, the presence of several dihedrals with two or more isomeric states and consequent events of barrier crossing slows down the relaxation time-scale of loop fluctuations.

For very large f_B ($f_B > 2k$),ω_n becomes imaginary so that there is no barrier re-crossing. The isomeric transitions in such cases are known as Kuhn mechanism [38–40] where dihedral hopping gets slower with increasing barrier height, in contrast to our observation. When a polypeptide or protein undergoes folding/unfolding, the dihedral angles show transitions among different isomeric states separated by such large barriers and are dominated by the Kuhn mechanism. The Kuhn mechanism can be recovered in our model considering the over-damped limit of Langevin equation [41]. In the large friction (over-damped) regime ignoring $I\ddot{\theta}$ term in our model we get $\tau \propto f_B$.

4. Discussions

Comparing the populations at different peaks of dihedral distributions in apo and holo-states, we find different patterns of changes in

Table 3
The percentage (%) of different isomerisation patterns: SP1, SP2 and MP observed for backbone dihedral angles of loop residues in different proteins.

	SP1%	SP2%	MP %
CaM Loop1	28.3	32.3	39.4
CaM Loop2	49	30	21
CaM Loop3	50	45.8	4.2
CaM Loop4	25.45	66.25	8.3
TnC Loop1	36.5	51	12.5
TnC Loop2	20.5	37.5	42
CALB Loop1	42.8	21.5	35.7
CALB Loop2	58.3	24.7	17
aLA Loop	30	60	10

populations. We denote overlapping single peaked distributions, like that of $p_{A103}{}^{CaM}(\varphi)$ (Fig. 2a) as SP1. Here the same isomeric state is populated in both apo- and holo-conformations. Unimodal distributions with large amount of peak shift between apo- and holo-states, like $p_{D65}{}^{TnC}(\psi)$ (Fig. 2b) is termed as SP2. In case of multi-peaked apo-state distribution, like $p_{D20}{}^{CaM}(\varphi)$, where holo-state population is unimodal and grows in vicinity of any apo-peak is denoted as MP (Fig. 2c). The MP cases may be viewed as population shift via isomeric transitions over barriers and typically have slower relaxation. The instances of different isomerisation patterns in different protein loops are summarized in Table 3. This reflects that different loops in the same protein show different degree of isomerisation patterns.

MP cases are much higher in loop 1 and loop 2 forming N-terminal domain than in loop 3 and loop 4 forming C-terminal of CaM. According to these observations, C-terminal binding will be faster than N-terminal binding. This is in qualitative agreement with experimental results [5,25]. The presence of multiple isomeric states is similar to that reported in peptide folding where peptides undergo changes in secondary structures [30,39,42,43]. In contrast to peptide folding, the secondary structures of the ion binding loops do not show any change. Thus the dihedral transitions do not necessarily depend on changes of secondary structural elements and appear to be ubiquitous.

Our study indicates that presence of multiple dihedral isomeric states from metal ion binding loop residues slows down fluctuations of the entire loop and in turn may also affect ion binding rates non-trivially. The rate of any chemical process in a solvent depends inversely on medium viscosity, known as the Stoke's behaviour [43,44]. However, experimentally determined rates of various bio-molecular processes [45–52] by varying solvent viscosity show marked deviations from the Stoke's law. Both experiments and simulations confirm similar deviation for folding rates of different proteins, peptides and polymer chains [30,39,42,43,53–57]. The microscopic understanding of such anomalous dependence of the rates on solvent viscosity is yet an open question. It would be interesting to investigate if the dihedral relaxations provide microscopic understanding of anomalous kinetics in various bio-molecular processes.

5. Conclusions

To summarize, our analysis shows presence of several backbone dihedrals of Ca^{2+} binding loop residues with multiple isomeric states, in the apo-form compared to the holo-form. The dihedral relaxation time varies inversely to the barrier height separating these isomeric states. Frequent barrier crossing events across small barriers separating isomeric states renders the dihedral relaxations slower. The slow dynamic responses of these microscopic variables contribute to slowing down of large-scale fluctuations as well. Our results may be useful to understand the microscopic basis of kinetics of various bio-molecular processes.

Conflicts of interests

There are no conflicts to declare.

Acknowledgements

SS thanks the University Grants Commission, India for research fellowship and acknowledges Amit Das for helpful discussions. JC and MG acknowledge the Department of Science and Technology, India for funding.

Appendix A. Supplementary data

Supplementary data to this article can be found online at https://doi.org/10.1016/j.bpc.2019.106207.

References

[1] S. Linse, A. Helmersson, S. Forsen, J Biol Chem 266 (13) (1991) 8050–8054.
[2] M. Ikura, G.M. Clore, A.M. Gronenborn, G. Zhu, C.B. Klee, A. Bax, Science 256 (5057) (1992) 632–638.
[3] J.F. Maune, K. Beckingham, S.R. Martin, P.M. Bayley, Biochemistry 31 (34) (1992) 7779–7786.
[4] S. Pedigo, M.A. Shea, Biochemistry 34 (4) (1995) 1179–1196.
[5] M.A. Shea, B.R. Sorensen, S. Pedigo, A.S. Verhoeven, Methods Enzymol 323 (2000) 254–301.
[6] B.J. Killian, J. Yundenfreund Kravitz, M.K. Gilson, J Chem Phys 127 (2) (2007) 024107.
[7] N. Trbovic, J.H. Cho, R. Abel, R.A. Friesner, M. Rance, A.G. Palmer 3rd., J Am Chem Soc 131 (2) (2009) 615–622.
[8] M.S. Marlow, J. Dogan, Nat Chem Biol 6 (5) (2010) 352–358.
[9] A. Das, J. Chakrabarti, M. Ghosh, Biophysical Journal 104 (6) (2013) 1274–1284.
[10] J.O. Wrabl, J. Gu, T. Liu, T.P. Schrank, S.T. Whitten, V.J. Hilser, Biophys Chem 159 (1) (2011) 129–141.
[11] A. Das, J. Chakrabarti, M. Ghosh, Chem Phys Lett 581 (2013) 91–95.
[12] A. Das, J. Chakrabarti, M. Ghosh, Mol Biosyst 10 (3) (2014) 437–445.
[13] S. Sikdar, J. Chakrabarti, M. Ghosh, Mol Biosyst 10 (12) (2014) 3280–3289.
[14] A. Das, S. Sikdar, M. Ghosh, J. Chakrabarti, J. Phys. 638 (1) (2015) 012013.
[15] S. Sikdar, J. Chakrabarti, M. Ghosh, Mol Biosyst 12 (2) (2016) 444–453.
[16] R. Chattopadhyaya, W.E. Meador, J Mol Biol 228 (4) (1992) 1177–1192.
[17] L.A. Svensson, E. Thulin, S. Forsen, J Mol Biol 223 (3) (1992) 601–606.
[18] N.J. Skelton, J. Kordel, W.J. Chazin, J Mol Biol 249 (2) (1995) 441–462.
[19] M.V. Vinogradova, D.B. Stone, G.G. Malanina, C. Karatzaferi, R. Cooke, R.A. Mendelson, R.J. Fletterick, Proc Natl Acad Sci U S A 102 (14) (2005) 5038–5043.
[20] E.D. Chrysina, K. Brew, K.R. Acharya, J Biol Chem 275 (47) (2000) 37021–37029.
[21] K. Beckingham, J Biol Chem 266 (10) (1991) 6027–6030.
[22] M. Kataoka, J.F. Head, A. Persechini, R.H. Kretsinger, D.M. Engelman, Biochemistry 30 (5) (1991) 1188–1192.
[23] S. Pedigo, M.A. Shea, Biochemistry 34 (33) (1995) 10676–10689.
[24] B.R. Sorensen, M.A. Shea, Biochemistry 37 (12) (1998) 4244–4253.
[25] W.S. VanScyoc, B.R. Sorensen, E. Rusinova, W.R. Laws, J.B. Ross, M.A. Shea, Biophys J 83 (5) (2002) 2767–2780.
[26] J.J. Yang, A. Gawthrop, Y. Ye, Protein Pept Lett 10 (4) (2003) 331–345.
[27] Z. Grabarek, J Mol Biol 359 (3) (2006) 509–525.
[28] J.L. Gifford, M.P. Walsh, H.J. Vogel, Biochem J 405 (2) (2007) 199–221.
[29] W.J. Chazin, Acc Chem Res 44 (3) (2011) 171–179.
[30] J.J. Portman, S. Takada, P.G. Wolynes, J Chem Phys 114 (11) (2001) 5082–5096.
[31] J.A. McCammon, B.R. Gelin, M. Karplus, Nature 267 (5612) (1977) 585–590.
[32] J.A. McCammon, M. Karplus, Proc Natl Acad Sci U S A 76 (8) (1979) 3585–3589.
[33] B.R. Brooks, C.L. Brooks 3rd, A.D. Mackerell Jr., L. Nilsson, R.J. Petrella, B. Roux, Y. Won, G. Archontis, C. Bartels, S. Boresch, A. Caflisch, L. Caves, Q. Cui, A.R. Dinner, M. Feig, S. Fischer, J. Gao, M. Hodoscek, W. Im, K. Kuczera, T. Lazaridis, J. Ma, V. Ovchinnikov, E. Paci, R.W. Pastor, C.B. Post, J.Z. Pu, M. Schaefer, B. Tidor, R.M. Venable, H.L. Woodcock, X. Wu, W. Yang, D.M. York, M. Karplus, J Comput Chem 30 (10) (2009) 1545–1614.
[34] S. Sikdar, M. Ghosh, M. De Raychaudhury, J. Chakrabarti, Chem Phys Lett 605 (2014) 103–107.
[35] J.C. Phillips, R. Braun, W. Wang, J. Gumbart, E. Tajkhorshid, E. Villa, C. Chipot, R.D. Skeel, L. Kale, K. Schulten, J Comput Chem 26 (16) (2005) 1781–1802.
[36] Y. Miao, J. Baudry, J.C. Smith, J.A. McCammon, Proteins 84 (4) (2016) 501–514.
[37] H. Watanabe, M. Elstner, T. Steinbrecher, J Comput Chem 34 (3) (2013) 198–205.
[38] W. Kuhn, H. Kuhn, Helv Chim Acta 28 (1945) 1533–1579.
[39] I. Echeverria, D.E. Makarov, G.A. Papoian, J Am Chem Soc 136 (24) (2014) 8708–8713.
[40] S.M. Avdoshenko, A. Das, R. Satija, G.A. Papoian, D.E. Makarov, Sci Rep 7 (1) (2017) 269.
[41] A.S. Bodrova, A.V. Chechkin, A.G. Cherstvy, H. Safdari, I.M. Sokolov, R. Metzler, Sci

Rep 6 (2016) 30520.
[42] J.C. Schulz, L. Schmidt, R.B. Best, J. Dzubiella, R.R. Netz, J Am Chem Soc 134 (14) (2012) 6273–6279.
[43] D. de Sancho, A. Sirur, R.B. Best, Nat Commun 5 (2014) 4307.
[44] W. Zheng, D. De Sancho, T. Hoppe, R.B. Best, J Am Chem Soc 137 (9) (2015) 3283–3290.
[45] B. Gavish, M.M. Werber, Biochemistry 18 (7) (1979) 1269–1275.
[46] W. Doster, Biophys Chem 17 (2) (1983) 97–103.
[47] A.P. Demchenko, O.I. Ruskyn, E.A. Saburova, Biochim Biophys Acta 998 (2) (1989) 196–203.
[48] K. Ng, A. Rosenberg, Biophys Chem 39 (1) (1991) 57–68.
[49] H. Oh-oka, M. Iwaki, S. Itoh, Biochemistry 36 (30) (1997) 9267–9272.
[50] T. Kleinert, W. Doster, H. Leyser, W. Petry, V. Schwarz, M. Settles, Biochemistry 37 (2) (1998) 717–733.
[51] C.J. Feng, R.V. Kedia, J.T. Hazzard, J.K. Hurley, G. Tollin, J.H. Enemark, Biochemistry 41 (18) (2002) 5816–5821.
[52] P. Sashi, A.K. Bhuyan, Biochemistry 54 (29) (2015) 4453–4461.
[53] S.A. Pabit, H. Roder, S.J. Hagen, Biochemistry 43 (39) (2004) 12532–12538.
[54] T. Cellmer, E.R. Henry, J. Hofrichter, W.A. Eaton, Proc Natl Acad Sci U S A 105 (47) (2008) 18320–18325.
[55] A. Soranno, B. Buchli, D. Nettels, R.R. Cheng, S. Muller-Spath, S.H. Pfeil, A. Hoffmann, E.A. Lipman, D.E. Makarov, B. Schuler, Proc Natl Acad Sci U S A 109 (44) (2012) 17800–17806.
[56] W. Yu, K. Luo, J Chem Phys 142 (12) (2015) 124901.
[57] A. Soranno, F. Zosel, H. Hofmann, J Chem Phys 148 (12) (2018) 123326.